A computational model of mapping in echolocating bats

A computational model of mapping in echolocating bats

Dieter Vanderelst[a,*], Herbert Peremans[b]

[a] *University of Cincinnati, Departments of Psychology, Biological Sciences, Electrical Engineering & Computing Systems, and Mechanical & Materials Engineering, Corry Blvd 47, 45221 Cincinnati.*
[b] *University Antwerp, Active Perception Lab, Koningstraat 8, 2000 Antwerp*

Abstract

Echolocating bats can navigate to salient places relying solely on their sonar system. Currently, much about the mechanism underlying sonar-based navigation in bats remains unknown, and no computational models of this ability have been proposed. In this paper, we propose a computational model of sonar-based navigation in bats. In particular, we advance a model explaining how bats could assemble a cognitive map from their environment using only their sonar readings. The model consists of a low-level obstacle avoidance loop that gives rise to stable and environment derived flight corridors, i.e. preferred pathways for bats flying through the environment, and a high-level mapping loop running on top of the low-level loop that combines local view information extracted from echo signals with local self-motion information to recognize previously visited places and memorize their spatial relationships. Using this model, we simulate a bat exploring unstructured environments while constructing a cognitive map using a biologically plausible algorithm. The model we propose allows the simulated bat to construct a global map of its flight paths through the environment without the bat ever reconstructing the 3D layout of the local environment from any of its received echo signals. Indeed, neither the obstacle avoidance strategy that guides the bat through space nor the mapping algorithm requires the 3D geometric structure of the environment to be accessible to the bat.

Keywords: Bats, Echolocation, Navigation, Chiroptera, Animal Movement, Obstacle Avoidance

*Corresponding author
Email addresses: vanderdt@ucmail.uc.edu (Dieter Vanderelst), herbert.peremans@uantwerpen.be (Herbert Peremans)

1. Introduction

Echolocating bats can navigate to salient places (Schnitzler et al., 2003) relying solely on their sonar system. Indeed, bats deprived of sight have been found to successfully return to their roost when displaced by up to 40 miles (Stones and Branick, 1969; Williams et al., 1966; Davis and Barbour, 1970; Mueller and Emlen, 1957). Also, bats exploring completely dark flight cages have been shown to retain spatial memory over long periods of time (Barchi et al., 2013). Moreover, as in other mammals (Derdikman and Moser, 2010), place cells have been found that encode the bat's location while echolocating (Yartsev and Ulanovsky, 2013; Ulanovsky and Moss, 2007). Currently, much about the mechanism underlying sonar-based navigation in bats remains unknown (Holland, 2007; Geva-Sagiv et al., 2015) and no computational models of this ability have been proposed.

In this paper, we advance a computational model explaining how bats could assemble a cognitive map representing the global layout of the flight corridors in their environment using only sonar readings. The concept of a cognitive map has been employed differently by various authors (Bennett, 1996). However, here we use its original definition as a global spatial representation of the animal's environment (Tolman, 1948). We propose the bat constructs first a topological map (Trullier et al., 1997; Franz and Mallot, 2000) representing only neighborhood relationships, i.e., a graph representation with nodes corresponding to distinct places and edges to specific motor programs, that is subsequently and gradually augmented with metric information, i.e., distances and directions, as the bat revisits the same distinct places. We have called such maps of the environment augmented topological maps (Peremans and Vanderelst, 2013) and referred to them as semi-metric maps because the accuracy of the metric information associated with the nodes varies across the graph. For less-traveled parts of the environment, the metric information can be unreliable, and the map is still mostly a topological map. For well-explored parts of the environment, the metric information can be used for optimizing paths: for instance, in calculating shortcuts. As such, the model presented here is intended to model bats engaged in 'middle-scale navigation' as introduced in (Schnitzler et al., 2003).

The proposed model is based on two assumptions. First, we assume that, while exploring a novel environment, purely reactive sensorimotor loops guide the bat (Vanderelst et al., 2015). Second, we assume that bats can recognize a place in the environment without reconstructing its local 3D spatial layout (Vanderelst et al., 2016). The first assumption is based on the observation that many bats when commuting between roosts and feeding grounds follow distinct routes along the edges of landscape structures traveling on flyways that show high spatial constancy (Holderied et al., 2006; Schaub and Schnitzler, 2007; Verboom, 1998; Schnitzler et al., 2003). In a previous paper (Vanderelst et al., 2015), we have presented a simple obstacle avoidance algorithm, capable of steering a bat

away from obstacles in both 2D and 3D environments. In addition to avoiding collisions, this mechanism also constrains the bat's movement through the environment causing it follow but a limited set of routes among all the possible ones through a given environment. The second assumption derives from the observation that the ability of cruising bats to reconstruct a 3D geometrical model of the local environment from sonar echoes is inherently limited by the (1) field of view (Surlykke et al., 2009; Jakobsen et al., 2013a,b), (2) update rate (Holderied et al., 2006; Seibert et al., 2013) and (3) temporal resolution of their sonar system (Simmons et al., 1989; Wiegrebe and Schmidt, 1996; Surlykke and Bojesen, 1996). As an alternative to 3D geometric reconstructions, we investigated the discriminative power of echo signatures extracted from a large body of sonar echoes collected in real bat habitats (Vanderelst et al., 2016). An echo signature is a biologically plausible range-energy representation of a sonar echo extracted by calculating the envelopes of the outputs of a cochlear filterbank, dechirping these outputs and summing over the frequency channels. In brief, an echo signature is a coarse range-energy (or, time-energy) representation of the echo. Our main result is then to show, using numerical simulations, how a robust mapping capability arises out of the interactions of this low-level reactive behavior with the echo signature based place recognition mechanism.

2. The mapping Model

A problem central to building a cognitive map (and navigation in general) is the fact that path integration measurements are typically noisy. If path integration (also referred to as odometry) were free of errors, building a cognitive map would be trivial since the ego-motion trace could be used directly to form a cognitive map of the environment (Thrun and Leonard, 2008). Unfortunately, both systematic and random errors accumulate rapidly (Thrun and Leonard, 2008; Merkle et al., 2006; Cheung and Vickerstaff, 2010) thereby prohibiting the direct use of the ego-motion. Therefore, building an accurate cognitive map requires an animal to have a method for correcting accumulated path integration errors.

In robotics, correcting path integration errors is usually done by averaging the noisy odometry estimates across subsequent travels between places (Thrun and Leonard, 2008). For large robots in confined spaces (or with long perceptual ranges, Williams et al., 2001) this has shown to be a feasible approach (e.g., Steckel and Peremans, 2013; Milford et al., 2004). The constraints imposed by the environment ensure the robot travels along a limited number of paths. This results in the robot encountering the same places multiple times. This allows the robot to accumulate a sufficient number of replications for a given path between two places. Over time, this leads to a faithful representation of the spatial relationship between places.

For small animals (or robots) this approach is problematic. However, small and agile navigators can follow many paths as the environment does not constrain the motion to the same degree as it does for larger agents. Therefore, it is not guaranteed that the agent will re-encounter the same places ever again. For echolocating bats, the issue is further aggravated by their limited perceptual range (Stilz and Schnitzler, 2012), the small aperture angle (Jakobsen et al., 2013b; Vanderelst et al., 2010) and the fact that echoes are aspect angle dependent (e.g., Yovel et al., 2009). This implies that, for a bat to recognize the echo signature as that from a place it has visited before, it has to be in a somewhat similar position and orientation than it was before. This is much less so for navigators with wide-aperture sensors, such as robots or insects with omnidirectional vision (Lambrinos et al., 2000).

In summary, mapping requires robust place recognition to integrate measurements across different encounters of the same places (Kuipers, 2000). Also, because echoes are highly dependent on the location and orientation of a bat, any mechanism that limits the possible positions and orientations of a bat would facilitate the construction of a cognitive map by guaranteeing the bat revisits the same places multiple times.

2.1. Place recognition

Navigating and route-following require animals to recognize previously visited places (Franz and Mallot, 2000; Trullier et al., 1997; Kuipers, 2000). While it is evident bats can identify places based on sonar (e.g., Barchi et al., 2013; Jensen et al., 2005), it is largely unknown how they do this (Schnitzler et al., 2003) and different mechanisms are possible (Geva-Sagiv et al., 2015). It has been suggested that bats make use of the reconstructed local 3D geometrical structure to recognize places (e.g., Lewicki et al., 2013; Clare and Holderied, 2015). While we agree that this hypothesis is sufficient to explain place recognition, we argue that it accounts insufficiently for the limitations of the bat sonar system. More importantly, it is not necessary.

As an alternative to the assumption that bats reconstruct the 3D layout of the environment, we recently proposed that bats directly use the cochlear output (Vanderelst et al., 2016), extending the template based classification approach described by Wiegrebe (2008) and Kuc (1997a,b,c). Under this hypothesis, bats are assumed to match the output of the cochlea to a set of stored templates, i.e., recognizing the echo signature of previously visited places, obviating the need for complex reconstruction algorithms extracting 3D spatial information from the echo signals at the two ears. As it uses the sensory input directly, this approach to place recognition is analogous to the view-based place recognition that is thought to underlie visual navigation in many insects (Zeil et al., 2003; Graham, 2010). In addition to circumventing the computationally hard problem of deriving a 3D

spatial representation from complex echo signals, robotic experiments have shown such acoustic templates to be highly discriminative (Steckel et al., 2013). In a convincing demonstration of the power of this approach, Kuc (1997c) showed a sonar device to be capable of detecting which side of a coin is up using simple echo templates.

In recent work (Vanderelst et al., 2016), we collected a large body of echo trains from a number of natural environments. Using a model of bat cochlear processing (Wiegrebe, 2008), we constructed biologically plausible templates. We found that these templates are also highly discriminable. Even the echoic templates from nearby places in the environment can be correctly classified. Therefore, templates can be used to recognize distinct places in the environment. Besides, nearby templates tend to resemble each other (more than templates from places further away). Thus, it is possible to recognize a given place even if the bat is not exactly in the same position and orientation a template was collected. Hence, our work characterizing real bat habitats (Vanderelst et al., 2016) and work in robotics (Steckel and Peremans, 2013; Kuc, 1997a,b,c) shows that acoustic templates can be used as a mechanism to recognize distinct places.

In summary, the mapping model presented in this paper assumes that bats can recognize different locations in the environment using their echo signature, as encoded in a template. As we have demonstrated empirically this is possible (Vanderelst et al., 2016; Steckel and Peremans, 2013), we do not model place recognition explicitly. Instead, we use the statistical properties of the previously recorded templates to parameterize the model (see below for details).

2.2. Path-constraining sensorimotor loops

Recently, we proposed an algorithm for obstacle avoidance in bats that relies on a very simple, yet robust, mechanism comparing the loudness of the onset of the echoes at the left and right ear and turning away from the side receiving the loudest echo (Vanderelst et al., 2015). This simple obstacle avoidance algorithm can steer the bat away from obstacles in both 2D and 3D environments. Importantly, the algorithm does not assume bats reconstruct the spatial layout of the obstacles from the echoes. As such, this algorithm is compatible with template based place recognition proposed in the previous section.

The obstacle avoidance algorithm highly constrained the movement through the environment causing the bat to follow a limited set of routes through a simulated given environment (See figs. 5, 8, 9 & 13 in Vanderelst et al., 2015). Therefore, this obstacle avoidance mechanism but also other environment-driven guidance behaviors (Geva-Sagiv et al., 2015), e.g., edge following (Verboom et al., 1999; Holderied et al., 2006), that make bats follow a restricted set of routes through the environment while exploring, could potentially allow bats to build a template based description of the environment. Note that several such guidance

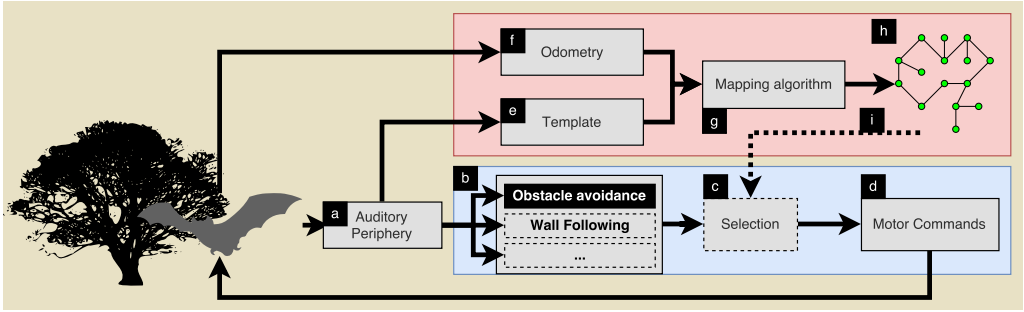

Figure 1: Illustration of the mapping model. Dashed boxes indicate parts of the model that have not been implemented in the current paper. Details in the text.

behaviors could be active simultaneously, each one driven by a particular sensorimotor loop transforming sensory input into motor commands (Brooks, 1986). A parallel control architecture along these lines has been proposed as a model of biological sensorimotor control (Mataric and Michaud, 2008; Brooks, 1986; Pfeifer and Bongard, 2006). In these controllers, a selection mechanism is used to ensure only a single sensorimotor loop provides input to the motor system at each point in time (Pirjanian, 1999).

In this paper, we only tested a single sensorimotor loop for its ability to support mapping. In particular, we re-implemented the obstacle avoidance mechanism we previously proposed (Vanderelst et al., 2015).

2.3. Model Functionality

Figure 1 illustrates the mapping model, combining (1) template based place recognition and (2) independent sensorimotor loops guiding the bat through the environment. Echoes received by the bat are processed by the auditory periphery (fig. 1, label a). The output of the cochlea is assumed to be processed by a number of independent sensorimotor loops (fig. 1, label b). Each of these generates a set of prospective motor commands steering the bat (fig. 1, label d). A selection mechanism (fig. 1, label c) is assumed to select one of the proposed motor commands to be executed. Note that, as we only implement obstacle avoidance in the current paper, no selection mechanism is required.

While the bat explores the environment, steered by the sensorimotor loops, it builds a database of acoustic templates identifying distinct places in the environment (fig. 1, label e). In combination with the (noisy) odometry information (fig. 1, label f), the database of templates is used by a mapping algorithm (fig. 1, label g) to construct a semi-metric map of the environment (fig. 1, label h). In our model, using the map for navigation would entail selecting the appropriate sensorimotor loops based on the map (fig. 1, label i). Thus, the selected sensorimotor loop would act as a local navigation strategy taking the bat to the

next location, where another loop might be selected (Franz and Mallot, 2000). However, in this paper we only model mapping.

3. Methods

3.1. Acoustics and arenas

Two-dimensional arenas with a radius of 25 meters were generated to test the mapping algorithm. Each of the 1 m^2 patches of the arena could be occupied by a single reflector. The reflectors were assumed to be vertical chains, a type of obstacle that has also been used in behavioral experiments (Barchi et al., 2013; Petrites et al., 2009).

The first step in generating an arena was to smooth (Garcia, 2010) an array of 50 $\times$ 50 elements containing random numbers. Each element of this array corresponds to a single patch in the arena. Next, a proportion p of the arena's patches corresponding to the array elements with the p proportion of highest values were populated with a reflector. We generated arenas with five different coverage levels p, i.e., from 10% to 50% in steps of 10 %. For each of the five coverage levels, 25 different arenas were generated.

The model we present is not species-specific. However, morphological and echolocation parameters are correlated across species of bats (e.g., Jones, 1999). Therefore, in the current paper, parameters for a single species are used to ensures that the combination of parameters is realistic. Thus, we modeled the echoes received by a bat flying through the arenas based on the parameters of the bat *Phyllostomus discolor* (Kwiecinski, 2006). This bat emits short frequency modulated pulses with a fundamental ranging from about 23 to 16 kHz (Schuchmann et al., 2005). However, most energy is usually contained in the 3rd-5th harmonics which range from about 45 to 100 kHz (Firzlaff and Schuller, 2003).

The strength of the echo in dB returning from each chain i was derived from measurements reported by Petrites et al. (2009). These authors ensonified plastic chains using FM sweeps from 110 to 15 kHz and measured the strength of the echoes returning for chains at distances between 0.23 and 1.42 meter. The chains used by Petrites et al. (2009) were composed of links 4.0 cm wide, 7.5 cm long, and 1.0 cm thick. Following a procedure used by Stilz and Schnitzler (2012), the measured echo strengths were used in the following linear regression,

$$\Delta L = C_1 + C_2 \cdot log_{10} \frac{r}{0.1} \tag{1}$$

with ΔL the loss in echo strength (with respect to the call intensity, in Decibels) and r the distance to the chain. In this equation, the parameters C_1 and C_2 represent the reflector strength and the spreading loss, respectively (Stilz and Schnitzler, 2012).

The values of ΔL were taken from the data as reported by Petrites et al. (2009) and corrected for atmospheric attenuation. The best fitting values for C_1 and C_2 were -6.59 and -12.34, respectively (see fig. 2). Hence, at each simulated call, equation 2 is used to determine the echo strength E_i of chain i at distance r_i and angle α_i

$$E_i = s_{bat} + d_{\alpha_i} - 6.59 - 12.34 \cdot log_{10}\frac{r_i}{0.1} + 2r_i a_f \tag{2}$$

In equation 2, s_{bat} is the strength of the call at 10 cm from the mouth, in this paper taken to be 110 dB_{SPL}. The parameter d_{α_i} gives the directional sensitivity of the sonar apparatus of the bat for angle α_i. The directional sensitivity of the bats sonar d_{α_i} was available from earlier simulation studies (Vanderelst et al., 2010; De Mey et al., 2008). The parameter a_f denotes the atmospheric attenuation. Instead of modeling a different atmospheric attenuation a_f for each frequency component of the call, a single attenuation of -2.37 $^{dB}/_{m}$ is used. This corresponds to average atmospheric attenuation across the interval 45-100 kHz (Bass et al., 1995).

3.2. Obstacle avoidance and simulated flights

In this paper, the bat is assumed to explore the arena steered only by obstacle avoidance. The obstacle avoidance strategy modeled here is identical to the strategy we proposed in our previous work (Vanderelst et al., 2015). It assumes the bat compares the amplitude of the onset of the echo trains in the left and the right ear. If the amplitude of the onset is higher in the left than in the right ear, the bat turns right (and *vice versa*).

The simulations used a fixed inter pulse interval of 100 ms. Thus, we modeled the bat emitting a call every 100 ms. We were unable to find data on the call rates used by *P. discolor*. However, data on other FM bats shows that 100 ms is a realistic interval for cruising bats flying in cluttered environments (Surlykke and Moss, 2000; Verboom et al., 1999). For each simulated call, the echo amplitudes (E_i, eq. 2) of the echoes received within 1 ms after the first detectable echo at each ear were summed,

$$L_x = \sum_{\forall E_i > 0} 10^{\frac{E_i}{20}} \tag{3}$$

This resulted in the amplitude of the echo train onset L_l and L_r at the left and the right ear, respectively. As indicated in equation 3, echoes with an amplitude E_i below 0 dB_{SPL} were disregarded in calculating L_l and L_r as they were considered to be undetectable. The hearing threshold for *P. discolor* has been measured using several methods (Reviewed by Hoffmann et al., 2008). The behavioral threshold, in the frequency range of the echolocation calls was found to be lower than 0 dB_{spl} (about -10 dB_{spl}, Hoffmann et al., 2008). However, a threshold of 0

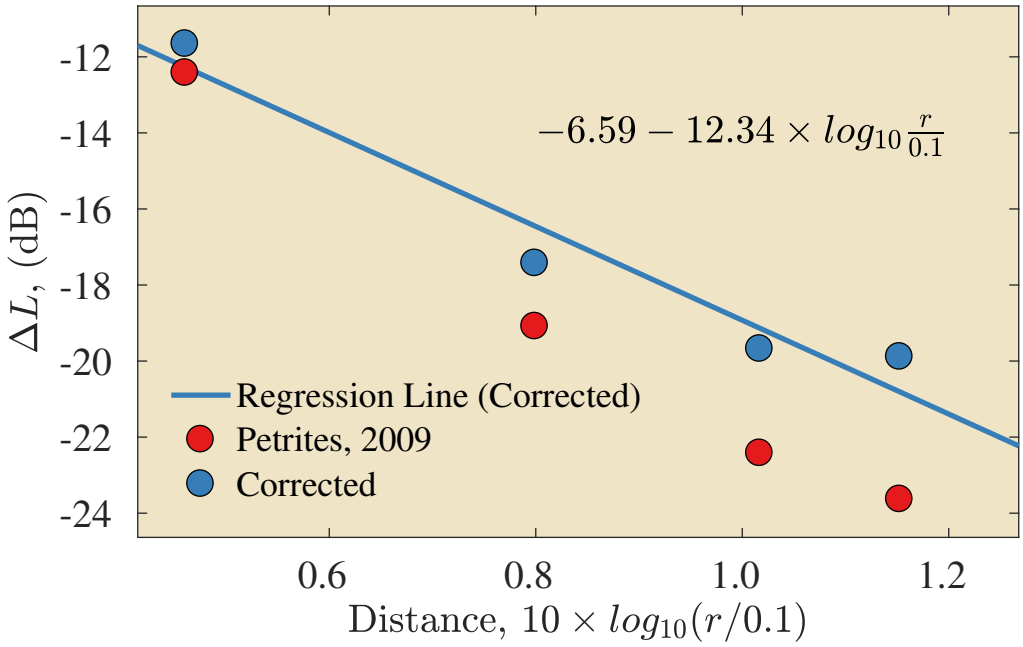

Figure 2: Determining the echo strength of the chains as a function of distance d. The red data points were taken from Petrites et al. (2009) and represent the echo strength (relative to the emission strength) recorded for plastic chains at various distances. We corrected the values for atmospheric attenuation assuming a perfectly flat spectrum in the range 20–60 kHz. This corresponds to the interval containing the most energy in the ensonification signals used by Petrites et al. (2009). The equation of the regression line – obtained using the procedure proposed by Stilz and Schnitzler (2012)– is shown in the graph.

dB$_{spl}$ was used in the model to account for the hearing threshold under natural conditions probably being higher than that measured in the lab.

The direction of rotation (left versus right) of the bat depended on the interaural level difference of the echo onsets. In addition, its rotational velocity was set based on the linear velocity of the bat. Hence, the new rotational velocity ω_r (in degrees per second) after call n was given by,

$$\omega_r = \begin{cases} +665 - 116 \cdot v_b & \text{if } L_r < L_l \\ -665 + 116 \cdot v_b & \text{if } L_r \geq L_l \end{cases} \tag{4}$$

with v_b the current flight speed. The flight speed of the bat v_b (in ms^{-1}) was updated after each call depending on the distance of the first detectable echo as follows,

$$v_b = \begin{cases} 0.3 + 0.94 \cdot \min_i(r_i) & \text{if } \min_i(r_i) < 5 \\ 5 & \text{if } \min_i(r_i) \geq 5 \end{cases} \tag{5}$$

with $\min_i(r_i)$ the distance to the nearest chains returning a detectable echo. Hence, the maximum speed of the bat was set to 5 ms^{-1}. For distances smaller than 5 m, the flight speed of the bat was linearly decreased to 0.3 ms^{-1} at a distance of 0 m. The parameters for setting both the flight speed and rotational velocity used here have been motivated in our previous paper (Vanderelst et al., 2015).

Note that eq. (3) does not take into account interference between echoes thereby possibly changing the relative strength of L_r and L_l (and therefore the sign of ω_r) for a certain proportion of the calls. To obtain an estimate of the probability of this happening we simulated the interference between 2 to 10 echoes using a model of bats auditory periphery (Wiegrebe, 2008) (See supporting material for details). This procedure resulted in an estimate of the probability $P(n)$ that interference changes the relative strength of L_r and L_l given n detectable echoes. Hence, as a phenomenological model of the effect of interference, we inverted for every call the sign of w_r with a probability $P(n)$ depending on the number of detectable echoes.

Ubernickel et al. (2013) found a reaction time of about 50 ms to transient targets in the trawling bat *Noctilio leporinus*. This agrees with a similar range of reaction times of 47-63 ms found by Melcón et al. (2007). Hence, we allowed for 50 ms to process the echoes. As such, the time interval Δt between the call emission and the start of the turn is the sum of (1) the time for the first echo to arrive, (2) a 1 ms interval over which the echoes are integrated, and (3) a 50 ms delay, modeling the reaction time. Therefore, Δt (in seconds) is equal to,

$$\Delta t = \frac{50 + 1}{1000} + \frac{2 \cdot \min_i(r_i)}{v_{sound}} \text{ with } v_{sound} = 344 \tag{6}$$

During this interval Δt, the current direction and speed of flight were maintained. After this interval, the bat rotated for the remainder of the inter pulse interval. If Δt was longer than 100 ms, the bat was not rotated. Hence, the (magnitude of the) angle θ rotated by the bat was given by,

$$\theta = \begin{cases} (0.1 - \Delta t) \cdot \omega_r & \text{if } \Delta t < 0.1 \\ 0 & \text{if } \Delta t \geq 0.1 \end{cases} \tag{7}$$

Likewise, the displacement s (meters) by the bat was given by,

$$s = \begin{cases} (0.1 - \Delta t) \cdot v_b + \Delta t \cdot v_b & \text{if } \Delta t < 0.1 \\ 0.1 \cdot v_b & \text{if } \Delta t \geq 0.1 \end{cases} \tag{8}$$

The simple algorithm outlined above was previously shown to steer free from obstacles in 2D and 3D environments (Vanderelst et al., 2015). However, the algorithm was not perfect at avoiding obstacles. Hence, we introduced a strategy to deal with near-collisions. Whenever the simulated bat detected an echo from a chain less than 1 meter away, it was turned around by 180°. As the chains were spaced 1 meter apart, this also guaranteed that the bat would not fly in between the chains. *P. discolor* has wing loading of about 13.6 N/m^2 (Giannini and Brenes, 2001). Based on the data of Aldridge (1987), the bat should be able to execute turns with a maximum curvature of about 20 m^{-1}, or with a radius of 5 cm. This agility allowed modeling the bat as being able to turn on the spot. It should be noted that, in comparison with many species, *P. discolor* has a high wing loading. Therefore, other species are able to perform even tighter turns (Aldridge, 1987).

We simulated the bat exploring each of the 25 arenas for each of the 5 coverage levels for 15 minutes in 5 flights of 3 minutes each (i.e., 1800 calls with an interpulse interval of 100 ms) – the bat was steered using the obstacle avoidance strategy described above. For each flight, the bat was returned to the starting position, i.e., the centre of the arena.

3.3. Modelled Odometry Errors

As the simulated bat explores the arenas, it is assumed to keep track of its position by path integration (Mittelstaedt and Mittelstaedt, 1982). In mammals, this is usually done by vestibular and kinaesthetic sensor systems (Seguinot et al., 1998) or visual information (e.g., Lappe et al., 2011). In bats, an additional system providing odometry information has been identified. Micro-hair cells covering the bat's wings detect changes in airflow providing information about its air speed (Sterbing-D'Angelo et al., 2011).

In animals, odometry estimates are confounded by both systematic and stochastic errors (e.g., Cheung and Vickerstaff, 2010; Merkle et al., 2006; Loomis et al.,

1999; Wolf, 2011; Seguinot et al., 1998). These have been studied in a range of organisms, including insects (e.g., Wolf, 2011; Müller and Wehner, 1988), mammals (Séguinot et al., 1993; Mittelstaedt and Mittelstaedt, 1982; Seguinot et al., 1998) and humans (Loomis et al., 1999; Lappe et al., 2011).

Many experiments have characterised the errors in homing after outward journeys consisting of a small number of straight legs. For journeys consisting of only 2 legs, models have been proposed that successfully predict the systematic errors (Müller and Wehner, 1988; Loomis et al., 1999; Merkle et al., 2006; Séguinot et al., 1993; Seguinot et al., 1998). Homing errors after longer and more complex journeys are not well described by these models. Hence, models that predict the systematic errors in path integration accumulated during long complex journeys are currently lacking (See Lappe et al., 2011, for an exception).

Fortunately, for the purpose of the current paper, we only need a model of the odometry errors for the short travels between a given recognized place i and the next place j. Indeed, the mapping algorithm described below only uses these pairwise odometry estimates in building a map. As will become clear in the next section, the distance travelled between two locations i and j is limited. Hence, the number of directional updates between i and j will be small and we can use the models and data describing odometry errors for short journeys.

3.3.1. Random Errors

Mittelstaedt and Mittelstaedt (1982) and Séguinot et al. (1993) reported on experiments with gerbils and hamsters returning to their nest after a straight outward path. To return home, the animals needed to perform a 180° turn. The mean angle turned by the animals corresponded very well with the required turn. However, the variability of the turns executed by the gerbils showed a 10-20° standard deviation. This corresponds to a standard deviation of 5-10% of the average turn of 180°. A similar value for the standard deviation was found for dogs turning by 90° on the outward path (Seguinot et al., 1998). Based on this convergency across species, we modeled the random noise on the registered turn as follows,

$$\hat{\theta} = \theta \cdot \varepsilon_\theta \text{ with } \varepsilon_\theta \sim \mathcal{N}(1, \sigma_{\varepsilon_\theta} = 0.1) \tag{9}$$

In equation 9, θ is the real angle turned by the bat (eq. 7) whereas $\hat{\theta}$ denotes the bat's own estimate of this turn angle. Likewise, some random error was imposed on the distance travelled. The variability (standard deviation) in the distance errors made by homing dogs was about 13% of travelled distance (Seguinot et al., 1998). Using this value, the random noise on the travel distance s (eq. 8) was modeled as follows,

$$\hat{s} = s \cdot \varepsilon_s \text{ with } \varepsilon_s \sim \mathcal{N}(1, \sigma_{\varepsilon_s}) \tag{10}$$

The true current heading direction φ_n of the bat (with respect to a coordinate system fixed to the arena) after the nth call was simply the sum of all rotations θ_k

(eq. 7) performed up to that point. Likewise, the absolute heading as estimated by the bat was obtained by summing all estimated rotations $\hat{\theta}_k$ (eq. 9). Hence,

$$\varphi_n = \sum_{k=1}^{n} \theta_k \text{ and } \hat{\varphi}_n = \sum_{k=1}^{n} \hat{\theta}_k \tag{11}$$

Similarly, the true total travel distance s_n after the nth call was simply the sum of all displacements performed up to that point and analogously for the estimated total travel distance

$$s_n = \sum_{k=1}^{n} s_k \text{ and } \hat{s}_n = \sum_{k=1}^{n} \hat{s}_k. \tag{12}$$

Finally, based on either φ_n, s_n or $\hat{\varphi}_n, \hat{s}_n$, the real and the estimated displacements in x and y were given by,

$$\Delta x_n = \cos\varphi_n \cdot s_n,\ \Delta y_n = \sin\varphi_n \cdot s_n \tag{13}$$

$$\Delta \hat{x}_n = \cos\hat{\varphi}_n \cdot \hat{s}_n,\ \Delta \hat{y}_n = \sin\hat{\varphi}_n \cdot \hat{s}_n \tag{14}$$

3.3.2. Systematic errors

In a seminal paper, Müller and Wehner (1988) presented data and a model capturing the errors made by homing desert ants. The same model has been successfully used to describe the behavior of golden hamsters in homing experiments (Séguinot et al., 1993). Merkle et al. (2006) showed that the predictions of this model can be explained parsimoniously by assuming that the animals' estimate of the travelled distance is kept track of by means of a leaky integrator, formalized in Cartesian coordinates by Lappe et al. (2011) as follows,

$$\Delta \hat{x}'_n = \frac{1 - e^{-\alpha \Delta \hat{x}_n}}{\alpha},\ \Delta \hat{y}'_n = \frac{1 - e^{-\alpha \Delta \hat{y}_n}}{\alpha} \tag{15}$$

In this equation, $\Delta\hat{x}$ and $\Delta\hat{y}$ are the noisy registered displacements in both the x and y-direction (eq. 14). The parameter α denotes the leakage rate, here set to 0.022 based on experiments with humans (Lappe et al., 2011). It should be noted that this leakage rate is higher than the rate found to best fit data from insects (i.e., $\alpha \sim 0.01$, Merkle et al., 2006). This agrees with the observation that mammals are less skilled path integrators than insects (Lappe et al., 2011; Seguinot et al., 1998).

3.3.3. Position estimate

The real x,y-position $P_n^\star$ of the bat after the nth call was given by,

$$P_n^\star = \left[\sum_{k=1}^{n} \Delta x_k \quad , \sum_{k=1}^{n} \Delta y_k \right] \tag{16}$$

Likewise, its own estimate of its position $\hat{P}_n$ as based on (the noisy) path integration as described above was given by,

$$\hat{P}_n = \left[\sum_{k=1}^{n} \Delta\hat{x}'_k \quad , \sum_{k=1}^{n} \Delta\hat{y}'_k \right] \tag{17}$$

containing both random (eq. 9 & 10) and systematic (eq. 15) errors. Note that for values of n that are multiples of 1800, both $P^{\star}_{n+1}$ and $\hat{P}_{n+1}$ are $[0, 0]$ as the bat was reset to the initial position after each 3 minutes flight (or 1800 calls). Likewise, both the true and estimated absolute orientation of the bat, φ and $\hat{\varphi}$ (eq. 11), were reset to 0 every 1800 calls.

Equations 9, 10 and 15 imply that, as the bat explores the arena, the accuracy of its position as estimated based on path integration (relatively to the origin) will deteriorate quickly. Both random and systematic errors in odometry will result in a (large) discrepancy between $\hat{P}_n$ and $P^{\star}_n$.

3.4. Mapping Algorithm

Several robotic algorithms have been proposed to build a map from inherently noisy odometry measurements (Thrun and Leonard, 2008) where the odometry measurements can be derived from both proprioceptive and exteroceptive sensors. Among these, the so-called Simultaneous Localization and Mapping (SLAM) algorithms exploit the fact that over small distances odometry estimates are more reliable than over large distances. Therefore, the estimate of the relative position of two nearby places i and j visited in succession will be fairly accurate. In brief, SLAM methods would, as an agent travels through space, assign each distinguishable place i, with real coordinates $P^{\star}_i$, a set of estimated coordinates $\hat{P}_i$, based on its current odometry-based position estimate $\hat{P}_o$. Over time, the reliability of the coordinates $\hat{P}_o$ estimated through path integration deteriorate. This will become apparent whenever the agent revisits a place i and the previously estimated coordinates $\hat{P}_i$ of this place deviate from the current odometry based estimate $\hat{P}_o$. In other words, the agent finds itself at a place i to which it has previously assigned coordinates $\hat{P}_i$ while its current path integration predicts it is at (the different) coordinates $\hat{P}_o$. SLAM methods allow resolving such inconsistencies and obtaining a reliable estimate of location coordinates $\hat{P}_i$ by integrating multiple noisy odometry measurements $\hat{P}_o$.

In the current paper, we assume the bat employs a biologically plausible SLAM algorithm to convert the noisy odometry information into a semi-metric map of the environment. The specific mapping algorithm used in this paper follows the general outline indicated above. In particular, the method we use is derived from RatSLAM, i.e., a bio-inspired mapping algorithm (e.g., Milford et al., 2004; Wyeth et al., 2011).

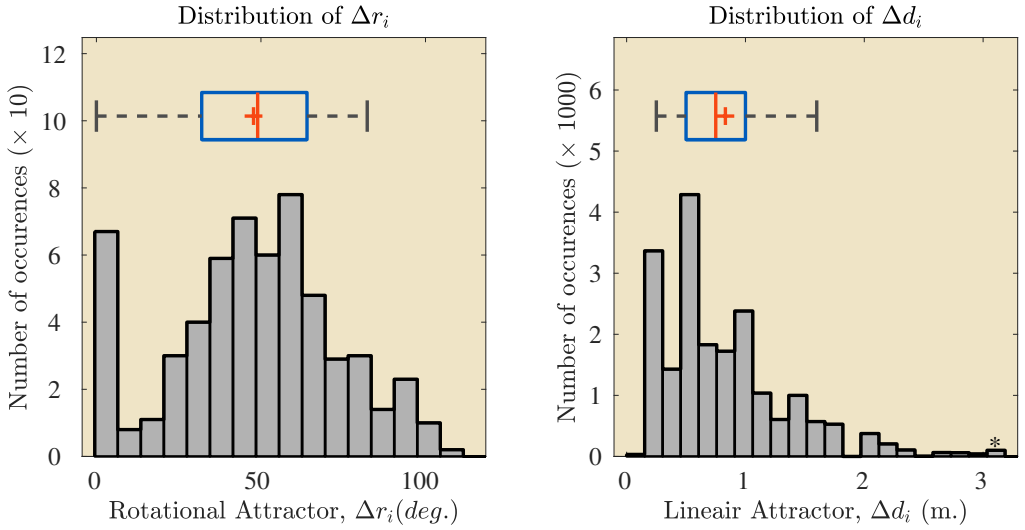

Figure 3: Distributions of Δd_i and Δr_i as used in this paper. These distributions were obtained by ensonifying real bat habitats as reported in previous work (Vanderelst et al., 2016). An asterisk ($\star$) above the bar indicated that it represents lumped data. Each panel features a boxplot of the data.

SLAM algorithms require that locations in the environment can be reliably recognized by the agent. In accordance with our robotic experiments (Steckel and Peremans, 2013) in an office environment, we assume the bat can use echolocation to recognize a place i it has visited before if it revisits the same location to within a distance of Δd meter. In addition, recognizing place i is assumed to require that the bat's orientation is similar to the orientation it had when first visiting location i. The maximum angular difference in orientation that still allows position i to be recognized is denoted by Δr.

In our simulations, the values of Δd and Δr were sampled for each place i from two empirically determined distributions (fig. 3) derived from previous work (Vanderelst et al., 2016). As mentioned above, we proposed template based place recognition might underlie sonar-based navigation in bats. Under this hypothesis, bats recognize places by remembering their echo signature - rather than their 3D layout. To test this hypothesis, we collected a large body of ensonification data in three different bat habitats. We proposed that the hypothetical templates could consist of a time-intensity profile derived directly from the cochlear output. Calculating such templates, we assessed their rotational and translational attractor regions. This is, we calculated for each template how far away and over what rotation the template could still be correctly classified. In effect, this data provides us with a distribution for Δd and Δr that can be used in the current paper.

While exploring the environment, guided by the obstacle avoidance sensorimotor loop described above, the bat updates its current estimated position $\hat{P}_o$ based on its estimated rotation $\hat{\theta}$ and speed $\hat{v}_b$ with each call. Next, it checks whether the current place i is in the set of places I that it has visited before. In other words, the bat checks whether it recognizes the current location. As stated above, the bat is assumed to recognize the current place if both of the following requirements are satisfied,

1. The current true position of the bat $P_n^\star$ differs by less than Δd_i from the true position $P_i^\star$ of location i.
2. The current true orientation of the bat φ_n differs by less than Δr_i degrees from the orientation it had when first encountering location i.

In case place i is not recognized, the bat memorizes place i as being newly visited (i.e., it adds i to set I) and assigns it the coordinates of its current estimated position $\hat{P}_o$ (fig. 4a),

$$\text{if } i \notin I : \hat{P}_o \rightarrow \hat{P}_i \tag{18}$$

In addition, values for Δd_i and Δr_i are sampled from the distributions (depicted in fig. 3) and associated with location i. Finally, the current orientation of the bat φ_n is stored as θ_i. Therefore, in the future, the bat will recognize position i if it approaches $P_i^\star$ to within less than Δd_i meter and with an orientation that differs by less than Δr_i degrees from the orientation θ_i it had when first encountering i. In other words, by sampling Δd_i & Δr_i and storing these values together with θ_i, the simulation sets up an attractor region around $P_i^\star$ inside of which the bat can recognize position i. It should be stressed that the bat has no access to either its own true location $P_n^\star$ or orientation φ_n. Neither does it have access to the true locations of the positions $P_i^\star$. If the bat encounters a location i that is recognized as a known place, the bat updates its own estimated location to the coordinates $\hat{P}_i$ associated with place i (fig. 4b), i.e.,

$$\text{if } i \in I : \hat{P}_o \leftarrow \hat{P}_i \tag{19}$$

This implies that the bat disregards the noisy odometry-based estimate of its current position $\hat{P}_o$ in favor of the estimated position for location i, $\hat{P}_i$. This is done because $\hat{P}_i$, as will be discussed in the next paragraph, is an estimate based on the integration of multiple estimates $\hat{P}_o$. As such, $\hat{P}_i$ will be generally more accurate than $\hat{P}_o$.

As said, SLAM algorithms provide methods for integrating multiple odometry-based estimates of a location's true position. In this paper, this is achieved by a so-called graph relaxation algorithm (Wyeth and Milford, 2009; Thrun and Leonard, 2008). After having travelled from a known place i to another known place j the bat stores an odometry based estimate of the displacement $\hat{O}_{ij}$ as

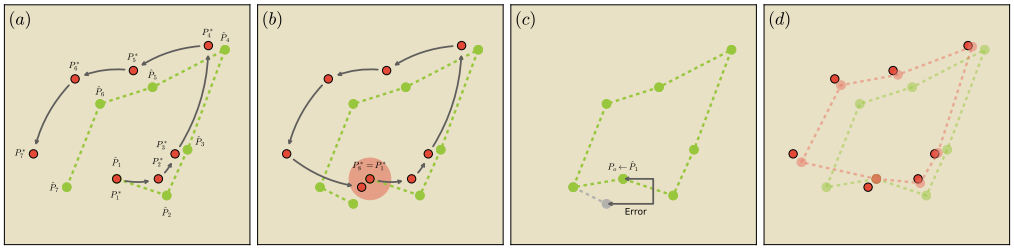

Figure 4: Illustration of the mapping process. (a) As the bat explores the environment, it adds new positions $\hat{P}_i$ to the set of known locations I (here, i ranges from 1 to 7). Due to accumulating odometry errors the distance between the real position P_i^* (red) and $\hat{P}_i$ (green) increases over time. In panel (b), the bat recognized the previously visited location P_1^*. The discrepancy between $\hat{P}_0$ (the bats current estimate of its own position) and $\hat{P}_1$ (the bats position of location 1) results in an error (panel c). The bat will set $\hat{P}_0$ to $\hat{P}_1$ (eq. 19). Next, in panel d, the error is taken into account by running the relaxation algorithm (eq. 20). This results in new position estimates for locations $\hat{P}_i$ (red line) that are closer to the true positions P_0^* (green line) than the original estimates $\hat{P}_i$ (red dots).

accumulated between positions i and j. After each call, the algorithm loops through all stored places i and updates the assigned coordinates as follows (fig. 4c-d),

$$\hat{P}_i \leftarrow \hat{P}_i + w \times [\Sigma_j(\hat{P}_i - \hat{P}_j - \hat{O}_{ij}) + \Sigma_k(\hat{P}_k - \hat{P}_i - \hat{O}_{ki})] \quad (20)$$

In equation 20, indices j indicate places the bat travelled to from location i. Indices k indicate places from which the bat travelled to location i. The parameter w governs the update rate and was set to 0.05. By iteratively applying equation 20, the relaxation algorithm attempts to increase the congruency between odometry based estimates and coordinate based estimates of displacements between known places (fig. 4d).

3.5. Random exploration

We assessed explicitly whether the obstacle avoidance behavior facilitated map formation. To this end, we altered the steering algorithm to behave randomly. At each call, the direction of turning (left or right) was chosen at random. Also, the flight speed was chosen randomly in the interval 0.3 to 5 ms^{-1}. As described above, the magnitude of the rotation was chosen based on flight speed (see eq. 5).

3.6. Evaluation of the map

The output of the mapping process described above is an estimated position $\hat{P}_i$ (with respect to the origin) for each location i in the set I. A defining feature

of semi-metric cognitive maps is their accurate representation of the distances between all mapped features, even if these are far apart. As such, a quantitative measure Q_m of the metric quality of the estimated locations $\hat{P}_i$ can be obtained by assessing the correlation between the pairwise distances for all places as mapped ($\hat{P}_i$) and in reality ($P_i^\star$),

$$Q_m = \mathrm{corr}_{ij}(|\hat{P}_i, \hat{P}_j|, |P_i^\star, P_j^\star|) \tag{21}$$

A high value Q_m indicates that the map has preserved the distances between places as they occur in the environment.

As odometry errors increase with the distance travelled, it can be expected that the cognitive maps will represent local relationships more accurately than global ones. To test whether this is the case, we use a second measure of quality Q_t.

To calculate Q_t, we first performed a non-rigid registration (Myronenko and Song, 2010) of the estimated positions $\hat{P}_i$ to the real positions $P_i^\star$ resulting in an updated set of estimated positions $\hat{P'}_i$ for the locations i in the set I. This registration does not conserve global distances and allows for global deformations of the map. However, it does conserve distances locally. The metric quality of these registered positions $\hat{P'}_i$ were then again assessed using the same correlation measure,

$$Q_t = \mathrm{corr}_{ij}(|\hat{P'}_i, \hat{P'}_j|, |P_i^\star, P_j^\star|) \tag{22}$$

The difference between Q_m and Q_t is an indication of how well the mapping algorithm preserves the global scale metric properties of the environment. If $Q_m \ll Q_t$, then some global deformations occurred in the construction of the cognitive map.

To judge the localization improvement due to mapping as such, the metric quality of the bat's own location estimates using path integration only, i.e., no mapping, was assessed by calculating the correlation between the pairwise distances for all bat locations as estimated ($\hat{P}_n$) and in reality ($P_n^\star$), resulting in the measure $Q_{p.i.}$,

$$Q_{p.i.} = \mathrm{corr}_{nm}(|\hat{P}_n, \hat{P}_m|, |P_n^\star, P_m^\star|) \tag{23}$$

Equation 23 is essentially the same as equation 21, without applying the mapping as described by equations 18, 19 and 20.

4. Results

4.1. Obstacle avoidance and resulting paths

A single example of the arenas for each level of coverage is given in figure 5. These figures also show the simulated paths of the bat. These plots show that, as in our previous work (Vanderelst et al., 2015), the obstacle avoidance algorithm was successful in steering the bat through the environment.

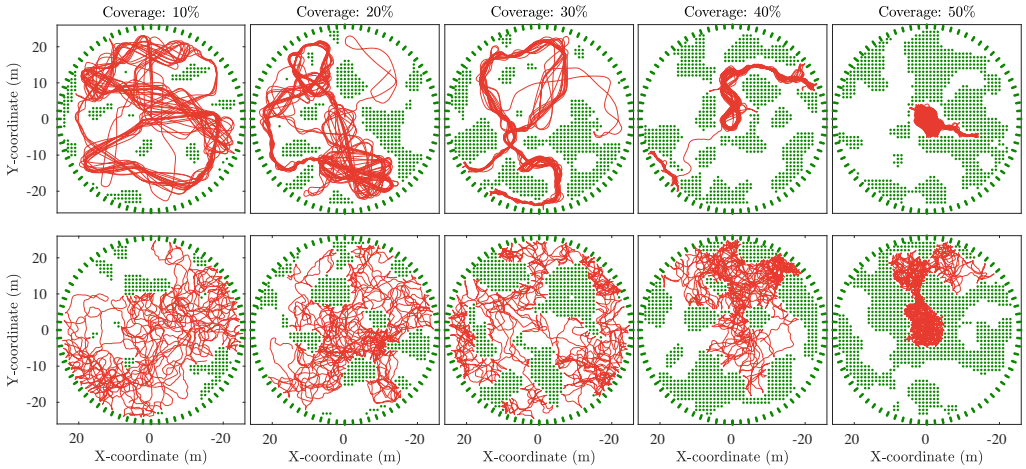

Figure 5: Examples of generated flight paths ($P_n^\star$, eq. 16) for a single replication for each of the 5 levels of coverage. Green dots are chains while the red lines depict the simulated flight path of the bat. In the top row panels, the bat was steered by the obstacle avoidance algorithm. In the bottom row, the obstacle avoidance algorithm was replaced by random exploration.

4.2. Use of space

We hypothesized that the obstacle avoidance algorithm would constrain the paths followed by the bat and limit the proportion of space used. Furthermore, we hypothesized that the positions would only be visited with a limited range of orientations (or headings). Therefore, we assessed what proportion of the state space is being used by the bat as a function of coverage. For each of the 25 replications and each of the 5 levels of coverage, we calculated a 3D (x-position $\times$ y-position $\times$ heading) histogram of the bat's position in space. The width of the bins in both the x and the y-direction was 1 meter. The bin width for the heading was 10 degrees. From this histogram, we calculated a cumulative histogram showing what proportion of the state space is occupied by the simulated bat (figure 6a). In calculating these cumulative histograms, bins containing a reflector or falling outside the arena were not counted. Figure 6a shows that the simulated bat, when steered using the obstacle avoidance mechanism, used only a fraction of the available space. Independent of the level of coverage, 90% of the time was spent in less than 10% of the available state space. When the obstacle avoidance algorithm was replaced by random exploration, the proportion of space used increased (Figure 6a). The increase in space use depended on the level of coverage (Figure 6b) and ranged from over 1.6$\times$ (10% coverage) to about 2.2$\times$ (50% coverage).

Importantly, using obstacle avoidance, the visited x,y-locations were typically associated with a narrow range of orientations. Using an arena with coverage 30% as example (fig. 6c), figures 6d-g show the distribution of orientations for a

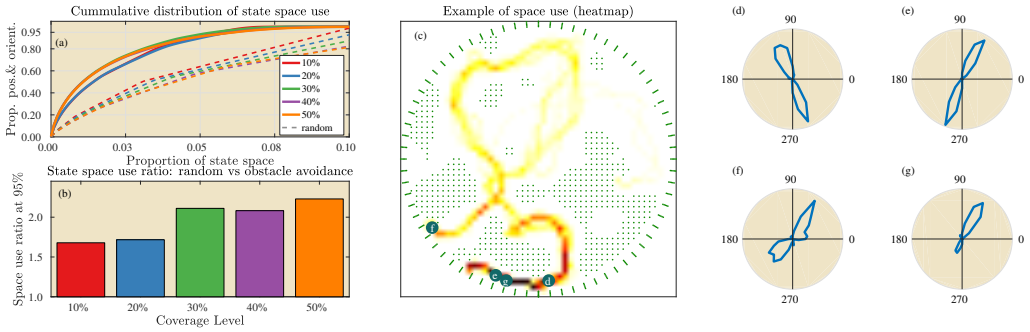

Figure 6: (a) Cumulative histogram indicating the proportion of the state space used by the simulated bats for each level of coverage (b) Comparison of the occupied proportion of the state space between the obstacle avoidance algorithm and a random exploration of the arena. (c) A heat map indicating the x,y-locations visited by a bat in an arena with coverage 30%. Darker colors indicate places that have been visited more often. (d)-(g) Four locations –with a high number of visits– have been selected (indicated with a green dot in (c)) for which the distributions of the orientations with which these locations were visited are shown.

number of x,y-positions. These highlight the narrow distribution of orientations associated with visited x,y-positions as well as its bi-modal nature (peaks separated 180 degrees). The latter is due to the bat travelling in approximately the same direction but opposite senses when passing through the selected positions.

4.3. Map Quality

Figure 7 shows examples of both the paths constructed by simple path integration (eq. 17) and the paths constructed by the mapping process (eqs. 18, 19 and 20) for each level of coverage. It is clear that simply using path integration does not lead to a useful representation of the paths through the environment. As a result, the mean correlations $\bar{Q}_{p.i}$ (eq. 23) between the estimated and the real distances range from about 0.60 to 0.70. Including a SLAM-like mechanism for recognizing places and updating their locations based on odometry information leads to a better representation of the paths through the environment. In particular, the structure of the environment is more faithfully extracted. This is reflected by the higher correlations between real and estimated distances. Depending on the level of coverage, the mean correlations $\bar{Q}_m$ (eq. 21) range from 0.92 to 0.96. For every level of coverage, the quality of the maps obtained by means of the mapping algorithm was significantly higher than that obtained through simple path integration, i.e., $\bar{Q}_m > \bar{Q}_{p.i}$ (fig. 8).

4.4. Random Exploration

Figure 9a depicts an example flight path resulting from replacing the default obstacle avoidance mechanism by the random exploration mechanism. Figure 9b

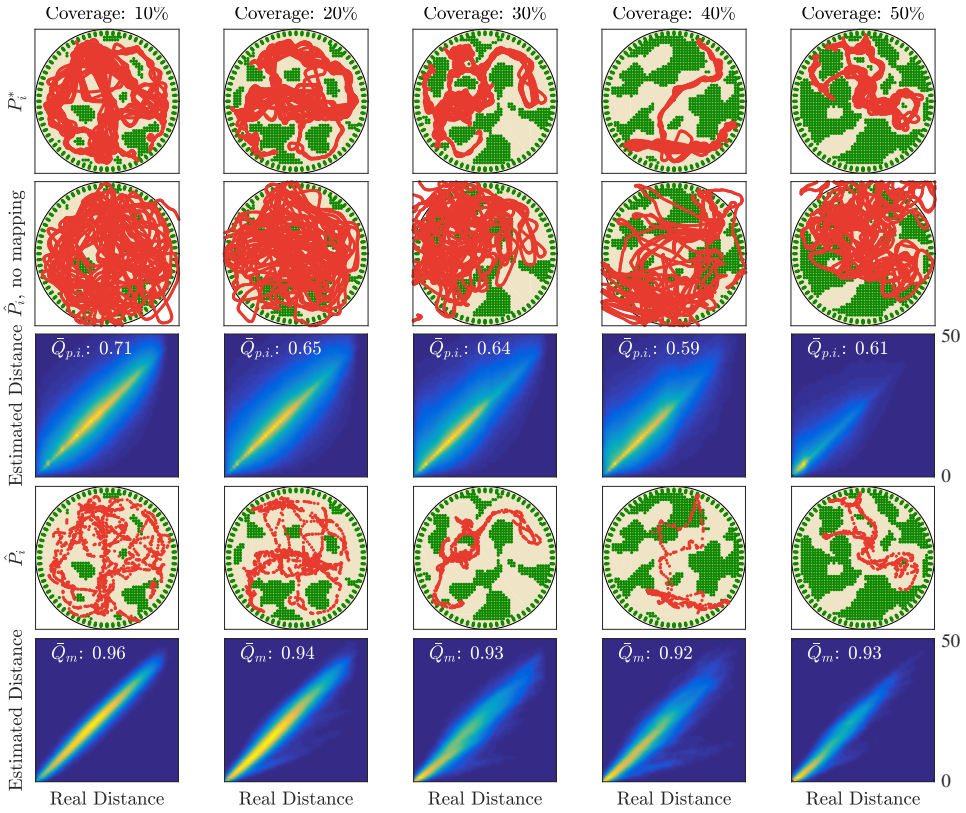

Figure 7: Examples of metric maps formed for each of the 5 levels of coverage. Top row: examples of true flight paths through the simulated environments (eq. 16). Second row: path integration based tracks (eq. 17) in the same environments. As can be seen, accumulated errors degrade the correspondence between the layout of the arena and the estimated path. Third row: histograms showing the correspondence between the distances as estimated using path integration and the real distances. These histograms have been calculated using the 25 replications for each coverage level. The mean correlation between the real and estimated distances is given in each panel. Fourth row: Estimated positions of each visited place (i.e., the locations $\hat{P}_i$) using the mapping SLAM algorithm. Fifth row: histograms showing the correspondence between the distances as estimated using the SLAM algorithm and the real distances. These histograms have been calculated using the 25 replications for each coverage level. The mean correlation between the real and estimated distances is given in each panel.

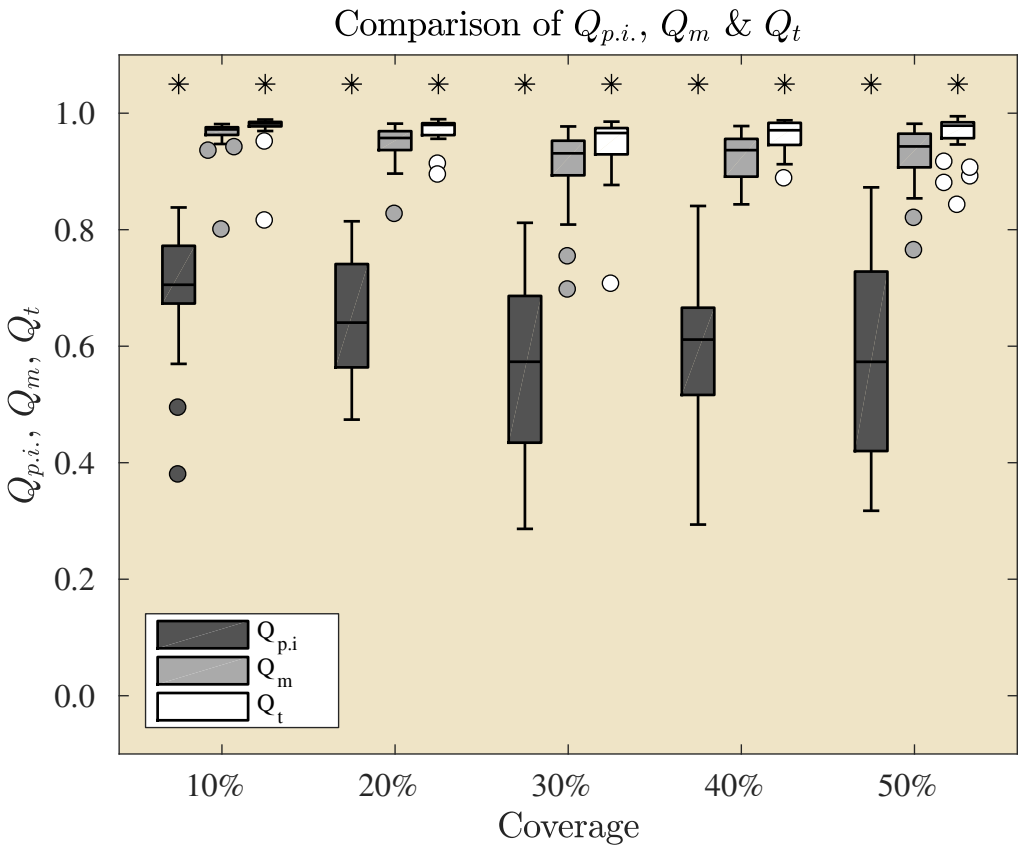

Figure 8: Boxplots of the quality for maps based on path integration ($Q_{p.i.}$, eq. 23) , SLAM (Q_m, eq. 21) and SLAM followed by a non-rigid transformation (Q_t, eq. 22), as a function of the coverage level. Asterisks above a box indicate a significant of the difference with the metric map quality (Kruskal-Wallis test, $p < 0.01$).

shows the reconstructed maps for both the SLAM mechanism ($\hat{P}_i$) and the SLAM mechanism followed by a non-rigid transformation ($\hat{P'}_i$). Comparing panels (a) and (b), it is clear that neither mapping procedure leads to a useful representation of the actual routes traveled. This is confirmed by the histograms depicting the correspondence between either $\hat{P}_i$ and $\hat{P}^\star{}_i$ (fig. 9c) and $\hat{P'}_i$ and $\hat{P}^\star{}_i$ (fig. 9d). Kruskal-Wallis tests confirmed that maps obtained through random exploration are less good than those obtained through the obstacle avoidance algorithm ($p \ll 0.01$).

4.5. Local map deformations

By allowing for a non-rigid registration between $P_i^\star$ and $\hat{P}_i$, we tested for local deformations in the reconstructed maps. Figure 10 illustrates the resulting

maps $\hat{P'}_i$ obtained after registering the positions $\hat{P}_i$ to the true positions $\hat{P^\star}_i$ by means of a non-rigid transformation. Depending on the level of coverage, the mean correlations $\bar{Q}_t$ (eq. 22) between the real distances and the estimated distances range from 0.94 to 0.97. For all levels of coverage, the quality of the map increased significantly by applying the non-rigid registration (i.e., $\bar{Q}_t > \bar{Q}_m$, fig. 8).

4.6. Sensitivity analysis

In the absence of data from bats, the model of the odometry noise (eqs. 9, 10 and 15) was parametrized using data on navigational errors in gerbils, hamsters (Mittelstaedt and Mittelstaedt, 1982; Séguinot et al., 1993) dogs (Seguinot et al., 1998) and humans (Lappe et al., 2011). We assessed to what extent our results are sensitive to the used parameter values by concurrently varying the parameters of equations 9, 10 and 15. We increased the values of $\sigma_{\varepsilon_\theta}$, σ_{ε_s} (the standard deviation of the random noise components) and α (the leakage parameter) by factors ranging from 1.25 to 2 in steps of 0.25.

For each noise level, we calculated the metric quality Q_m of the resulting maps (eq. 21. Figure 11 shows that, as the noise levels increase, the median map quality decreases. In addition, the variability of map quality increases. This is to be expected as, at least for the random noise, increased noise levels are defined as higher levels of variability in the odometry distance and angular estimates. Example of reconstructed maps are depicted in figure 11.

Figure 11 also displays the quality of the maps based on path integration alone, i.e. $Q_{p.i}$ (eq. 23). The increased noise levels directly degrade the precision of the path integration. Therefore, it is not suprising that the quality measure $Q_{p.i}$ is greatly reduced with increasing levels of noise. Importantly, these results also show that, even for increased noise levels, the quality of the maps as reconstructed using a biological plausible SLAM mechanism is better than the spatial representation obtained through pure path integration (even for the lowest noise level). This is, $Q_m > Q_{p.i}$, even when $Q_{p.i}$ is based on the lowest noise. Kruskal-Wallis tests confirmed this for every coverage level and every noise level ($p \ll 0.01$).

5. Discussion

In this paper, we simulated a bat exploring unstructured environments while constructing a cognitive map using a biologically plausible algorithm. The mapping (fig. 1) model we propose allows the simulated bat to construct a global map of its flight paths through the environment without the bat ever reconstructing the 3D layout of the local environment from any of its received echo signals. Indeed, neither the obstacle avoidance strategy that guides the bat through space

nor the mapping algorithm requires the 3D geometric structure of the environment to be accessible to the bat.

According to the mechanism described here this cognitive map first starts out as a topological map containing information about what paths can be followed to get from one recognizable location in the environment to another (Peremans and Vanderelst, 2013). While metric relationships between these different recognizable locations are assumed to be memorized from the start, they contain errors of such magnitude that this information can not be relied upon. However, even a purely topological map containing only information about recognizable locations in the environment and traversable pathways between them would already seem sufficiently powerful to support most if not all of the 'middle-scale navigation' described by Schnitzler et al. (2003). Indeed, topological maps are likely to support navigation in many animals (Trullier et al., 1997; Franz and Mallot, 2000; Bennett, 1996).

As the simulated bat grows more familiar with the environment, it incrementally refines the metric information stored with the recognizable locations thereby turning the topological map gradually into a locally metric map. Indeed, the results presented show that after more extensive exploration of the environment the resulting maps (positions $\hat{P}_i$) reflect the metrics of the local layout of the actual flight paths (positions P_i^*) quite well with correlations $\bar{Q}_m$ ranging between 0.93 and 0.96. The pair-wise distances are much more accurate than those obtained using path integration only ($\bar{Q}_{p.i.} \ll \bar{Q}_m$, fig. 8). Nevertheless, these maps are only semi-metric, i.e. locally metric, as some global deformations are usually present. This is indicated by the finding that non-rigid transformations of the map increase their quality $\bar{Q}_m < \bar{Q}_t$.

Based on robotic experiments (Steckel et al., 2008; Milford and Schulz, 2014) and theoretical analysis (Veelaert and Peremans, 1999), we hypothesize that, given sufficient time to explore the environment, the global deformations of the map would eventually disappear as well. In further support of this claim, we show in fig. 12(a) that more passes between two locations i and j in the simulations presented here result in a better representation of the distance between these positions.

Learning a map, according to the mapping mechanism proposed here, then requires regularly revisiting the same locations. Regularly revisiting of the same locations is facilitated by making the bat's trajectory through its environment depend upon that same environment. There is ample evidence that real bats show such guidance behavior when engaged in middle-scale navigation (Verboom, 1998; Verboom et al., 1999). Indeed, it is concluded by Schaub and Schnitzler (2007), based on observations of bats commuting between roost and hunting grounds, that regularly used flyways along linear landscape elements are advantageous for bats because they provide landmarks and contours for orientation, thus enabling

bats to fly faster in a familiar situation, and reduce predation pressure. Similarly, Holderied et al. (2006) found whiskered bats to follow highly constrained routes when flying along a forest corridor. Finally, Barchi et al. (2013) recently reported big brown bats to adopt – and remember – highly stereotypical flights paths through a flight room populated with obstacles. This has also been found in the field experiments reported by Kong et al. (2016).

We would like to point out that the analysis presented here shows that limiting the use of space to such a set of highly stereotyped flight paths would have the additional benefit of maximizing the probability of revisiting the same locations thereby leading to high-quality maps.

To illustrate that the flight paths generated by guidance behaviors as opposed to random exploration induced ones improve mapping, we have introduced a simple obstacle avoidance behavior. Qualitatively, it can be seen from the paths plotted in figure 5 that the obstacle avoidance mechanism leads to more restricted flight paths. Comparing the use of the state space (i.e., position and orientation) quantitatively (fig. 6), it is found that the obstacle avoidance algorithm restricts the proportion of the state space used by the bat. In particular, random exploration results in occupying up to about 2.2 times the number of states of obstacle avoidance based steering. The obstacle avoidance constrains both the x,y-position and the orientations occupied (fig. 6c-g). This leads to more passes between particular pairs of positions i and j (fig. 12b). As predicted, the spatial restrictions imposed by the obstacle avoidance behavior increase the accuracy of the extracted maps (fig. 9). Qualitatively, the inaccuracies resulting from a random flight path can be appreciated by inspecting fig. 9b. Statistically, the quality parameters differ significantly between maps reconstructed based on random paths and paths based on obstacle avoidance 9c & d.

While, in robotics, (cognitive) maps are usually considered as the only reliable navigation mechanism, biologists have pointed out that cognitive maps are not necessary for reliable navigation (See Franz and Mallot, 2000; Bennett, 1996; Trullier et al., 1997; Cheung et al., 2014, for discussions and references). It has even been questioned whether humans are capable of building cognitive maps of complex environments (Maurer and Séguinot, 1995). As such, the ability of bats to remember flight routes and returning to roosting places based on echolocation (Stones and Branick, 1969; Williams et al., 1966; Barchi et al., 2013) can not be taken as sufficient evidence of them having a cognitive map. Indeed, positively demonstrating that animals use a cognitive map is notoriously difficult (Bennett, 1996) as illustrated by the long-standing discussion about cognitive maps in insect navigation (Cheung et al., 2014).

Presenting a taxonomy of navigation strategies, Franz and Mallot (2000) lists two (non-local) navigation strategies that are simpler than cognitive maps. First, animals can navigate to a goal outside their perceptual range by chaining

stimulus-triggered responses into a fixed route (See also Trullier et al., 1997). Under this scheme, perceptual input triggers a behavioral response that leads the animal to the next location, where a new response can be triggered. This is the navigation strategy hypothesized to underlie route learning in many insects (e.g., Graham, 2010). Importantly, this navigation scheme does not allow for multiple routes to be integrated. The navigator can learn multiple routes, each of which can pass through the same locations. However, at each location only a single response can be elicited, depending on the currently activated route. Naturally, this scheme can be expanded to merge different routes leading through the same locations into a single graph with nodes representing locations. In this scheme, the edges leaving each node represent the different responses that can be elicited at this location leading to new locations (nodes). This constitutes the second navigation strategy, more simple than cognitive maps, listed by Franz and Mallot (2000) as topological navigation.

As said, these simpler alternatives to cognitive maps can currently not be ruled out in bats, nor in many other animals (Bennett, 1996; Moeser, 1988; Cheung et al., 2014). However, by demonstrating that bats, at least in principle, have access to the information necessary for building cognitive maps, we have demonstrated that both other simpler strategies can be supported by echolocation as well. Indeed, the use of cognitive maps as described here is essentially a topological navigation strategy that assigns (increasingly more accurate) metric coordinates to recognizable places. In turn, topological navigation is a variety of navigation using chained stimulus-response sequences, each response triggered by the recognition of a particular place. As such, we conclude that the assumptions on which our mapping model is based are sufficient to explain sonar-based navigation in bats, either using a cognitive map or some simpler strategy.

References

H.-U. Schnitzler, C. F. Moss, A. Denzinger, From spatial orientation to food acquisition in echolocating bats, Trends in Ecology & Evolution 18 (8) (2003) 386–394.

R. C. Stones, L. P. Branick, Use of hearing in homing by two species of Myotis bats, Journal of Mammalogy 50 (1) (1969) 157–160.

T. C. Williams, J. M. Williams, D. R. Griffin, The homing ability of the neotropical bat Phyllostomus hastatus, with evidence for visual orientation, Animal behaviour 14 (4) (1966) 468–473.

W. H. Davis, R. W. Barbour, Homing in blinded bats (Myotis sodalis), Journal of Mammalogy 51 (1) (1970) 182–184.

H. Mueller, J. Emlen, Homing in bats, Science 126 (3268) (1957) 307–308.

J. R. Barchi, J. M. Knowles, J. A. Simmons, Spatial memory and stereotypy of flight paths by big brown bats in cluttered surroundings, The Journal of experimental biology 216 (6) (2013) 1053–1063.

D. Derdikman, E. I. Moser, A manifold of spatial maps in the brain, Trends Cogn. Sci. (Regul. Ed.) 14 (12) (2010) 561–569.

M. M. Yartsev, N. Ulanovsky, Representation of three-dimensional space in the hippocampus of flying bats., Science 340 (6130) (2013) 367–372.

N. Ulanovsky, C. F. Moss, Hippocampal cellular and network activity in freely moving echolocating bats, Nature neuroscience 10 (2) (2007) 224–233.

R. a. Holland, Orientation and navigation in bats: Known unknowns or unknown unknowns?, Behavioral Ecology and Sociobiology 61 (2007) 653–660, ISSN 03405443.

M. Geva-Sagiv, L. Las, Y. Yovel, N. Ulanovsky, Spatial cognition in bats and rats: from sensory acquisition to multiscale maps and navigation, Nature Reviews. Neuroscience 16 (2) (2015) 94–108.

A. T. D. Bennett, Do animals have cognitive maps?, The Journal of experimental biology 199 (1) (1996) 219–224, ISSN 0022-0949.

E. C. Tolman, Cognitive maps in rats and men., Psychological review 55 (4) (1948) 189–208, ISSN 0033-295X.

O. Trullier, S. I. Wiener, A. Berthoz, J. arcady Meyer, Biologically Based Artificial Navigation Systems: Review And Prospects, Progress in Neurobiology 51 (5) (1997) 483–544, ISSN 0301-0082.

M. O. Franz, H. a. Mallot, Biomimetic robot navigation, Robotics and Autonomous Systems 30 (1-2) (2000) 133–153, ISSN 09218890.

H. Peremans, D. Vanderelst, Augmented topological maps for three-dimensional navigation., Behavioral and Brain Sciences 36 (5) (2013) 560–1; discussion571–87.

D. Vanderelst, M. W. Holderied, H. Peremans, Sensorimotor Model of Obstacle Avoidance in Echolocating Bats., PLoS Comput Biol 11 (10) (2015) e1004484.

D. Vanderelst, J. Steckel, A. Boen, M. Holderied, H. Peremans, Place recognition using batlike bio-sonar, eLife .

M. W. Holderied, G. Jones, O. von Helversen, Flight and echolocation behaviour of whiskered bats commuting along a hedgerow: range-dependent sonar signal design, Doppler tolerance and evidence for 'acoustic focussing'., Journal of Experimental Biology 209 (Pt 10) (2006) 1816–1826.

A. Schaub, H.-U. Schnitzler, Flight and echolocation behaviour of three vespertilionid bat species while commuting on flyways, Journal of Comparative Physiology A 193 (12) (2007) 1185–1194.

B. Verboom, The use of edge habitats by commuting and foraging bats., 10, IBN-DLO, 1998.

A. Surlykke, K. Ghose, C. Moss, Acoustic scanning of natural scenes by echolocation in the big brown bat, Eptesicus fuscus, Journal of Experimental Biology 212 (7) (2009) 1011.

L. Jakobsen, S. Brinklø v, A. Surlykke, Intensity and directionality of bat echolocation signals., Frontiers in physiology 4 (April) (2013a) 89, ISSN 1664-042X.

L. Jakobsen, J. Ratcliffe, A. Surlykke, Convergent acoustic field of view in echolocating bats, Nature 493 (7430) (2013b) 93–6.

A.-M. Seibert, J. C. Koblitz, A. Denzinger, H.-U. Schnitzler, Scanning behavior in echolocating common pipistrelle bats (Pipistrellus pipistrellus)., PLoS One 8 (4) (2013) e60752.

J. A. Simmons, E. G. Freedman, S. B. Stevenson, L. Chen, T. J. Wohlgenant, Clutter interference and the integration time of echoes in the echolocating bat, Eptesicus fuscus, The Journal of the Acoustical Society of America 86 (4) (1989) 1318–1332.

L. Wiegrebe, S. Schmidt, Temporal integration in the echolocating bat, Megaderma lyra, Hearing Research 102 (1) (1996) 35–42.

A. Surlykke, O. Bojesen, Integration time for short broad band clicks in echolocating FM-bats (Eptesicus fuscus), Journal of Comparative Physiology A 178 (2) (1996) 235–241.

S. Thrun, J. J. Leonard, Simultaneous localization and mapping, in: Springer handbook of robotics, Springer, 871–889, 2008.

T. Merkle, M. Rost, W. Alt, Egocentric path integration models and their application to desert arthropods, Journal of Theoretical Biology 240 (3) (2006) 385–399, ISSN 00225193.

A. Cheung, R. Vickerstaff, Finding the way with a noisy brain, PLoS Computational Biology 6 (11) (2010) 9–13, ISSN 1553734X.
S. Williams, G. Dissanayake, H. Durrant-Whyte, Towards terrain-aided navigation for underwater robotics, Advanced Robotics 15 (5) (2001) 533–549.
J. Steckel, H. Peremans, BatSLAM: Simultaneous Localization and Mapping Using Biomimetic Sonar, PloS one 8 (1) (2013) e54076.
M. J. Milford, G. F. Wyeth, D. Prasser, RatSLAM: a hippocampal model for simultaneous localization and mapping, in: Robotics and Automation, 2004. Proceedings. ICRA'04. 2004 IEEE International Conference on, vol. 1, IEEE, 403–408, 2004.
W. Stilz, H. Schnitzler, Estimation of the acoustic range of bat echolocation for extended targets, The Journal of the Acoustical Society of America 132 (3) (2012) 1765–75.
D. Vanderelst, F. De Mey, H. Peremans, I. Geipel, E. Kalko, U. Firzlaff, What noseleaves do for fm bats depends on their degree of sensorial specialization, PloS one 5 (8) (2010) e11893.
Y. Yovel, P. Stilz, M. O. Franz, A. Boonman, H. U. Schnitzler, What a plant sounds like: The statistics of vegetation echoes as received by echolocating bats, PLoS Computational Biology 5 (7), ISSN 1553734X.
D. Lambrinos, R. Möller, T. Labhart, R. Pfeifer, R. Wehner, A mobile robot employing insect strategies for navigation, Robotics and Autonomous systems 30 (1) (2000) 39–64.
B. Kuipers, The spatial semantic hierarchy, Artificial Intelligence 119 (1) (2000) 191–233.
M. E. Jensen, C. F. Moss, A. Surlykke, Echolocating bats can use acoustic landmarks for spatial orientation, Journal of experimental biology 208 (23) (2005) 4399–4410.
M. S. Lewicki, B. a. Olshausen, A. Surlykke, C. F. Moss, Scene analysis in the natural environment, Frontiers in Psychology 1 (2013) 0, ISSN 16641078.
E. L. Clare, M. W. Holderied, Acoustic shadows help gleaning bats find prey, but may be defeated by prey acoustic camouflage on rough surfaces, eLife 4 (2015) e07404, ISSN 2050-084X.
L. Wiegrebe, An autocorrelation model of bat sonar, Biological Cybernetics 98 (6) (2008) 587–595.
R. Kuc, Biomimetic sonar recognizes objects using binaural information, The Journal of the Acoustical Society of America 102 (1997a) 689.
R. Kuc, Biomimetic sonar locates and recognizes objects, IEEE Journal of Oceanic Engineering 22 (4) (1997b) 616–624.
R. B. Kuc, Biomimetic sonar differentiates coin head from tail, The Journal of the Acoustical Society of America 101 (1997c) 3198.
J. Zeil, M. I. Hofmann, J. S. Chahl, Catchment areas of panoramic snapshots in outdoor scenes., Journal of the Optical Society of America A 20 (3) (2003) 450–469, ISSN 1084-7529.
P. Graham, Insect Navigation, Encyclopedia of Animal Behavior 2 (2010) 167–175.
J. Steckel, A. Boen, H. Peremans, Broadband 3-D Sonar System Using a Sparse Array for Indoor Navigation, IEEE Transactions on Robotics 29 (1) (2013) 161–171.
B. Verboom, A. M. Boonman, H. J. G. a. Limpens, Acoustic perception of landscape elements by the pond bat (Myotis dasycneme), Journal of Zoology 248 (1) (1999) 59–66, ISSN 09528369.
R. A. Brooks, A robust layered control system for a mobile robot, Robotics and Automation, IEEE Journal of 2 (1) (1986) 14–23.
M. Mataric, F. Michaud, Behavior-Based Systems, in: B. Siciliano, O. Khatib (Eds.), Springer Handbook of Robotics, Springer Berlin Heidelberg, ISBN 978-3-540-23957-4, 891–909, 2008.
R. Pfeifer, J. Bongard, How the body shapes the way we think: a new view of intelligence, MIT press, 2006.
P. Pirjanian, Behavior coordination mechanisms-state-of-the-art, Tech. Rep., Citeseer, 1999.
A. E. Petrites, O. S. Eng, D. S. Mowlds, J. A. Simmons, C. M. Delong, Interpulse interval modulation by echolocating big brown bats (Eptesicus fuscus) in different densities of obstacle clutter, Journal of Comparative Physiology A: Neuroethology, Sensory, Neural, and Behavioral Physiology 195 (2009) 603–617, ISSN 03407594.

D. Garcia, Robust smoothing of gridded data in one and higher dimensions with missing values, Computational Statistics & Data Analysis 54 (4) (2010) 1167–1178.
G. Jones, Scaling of echolocation call parameters in bats, Journal of Experimental Biology 202 (23) (1999) 3359–3367.
G. G. Kwiecinski, Phyllostomus discolor, Mammalian Species 801 (2006) 1–11, ISSN 0076-3519.
M. Schuchmann, M. Hübner, L. Wiegrebe, The absence of spatial echo suppression in the echolocating bats Megaderma lyra and Phyllostomus discolor, Journal of Experimental Biology 209 (1) (2005) 152–157, ISSN 0022-0949.
U. Firzlaff, G. Schuller, Spectral Directionality Of The External Ear Of The Lesser Spear Nosed Bat Phyllostomus Discolor, Hearing research 181 (1-2) (2003) 27–39.
F. De Mey, J. Reijniers, H. Peremans, M. Otani, U. Firzlaff, Simulated head related transfer function of the phyllostomid bat Phyllostomus discolor, The Journal of the Acoustical Society of America 124 (4) (2008) 2123–2132.
H. Bass, L. Sutherland, A. Zuckerwar, D. Blackstock, D. Hester, Atmospheric absorption of sound: Further developments, The Journal of the Acoustical Society of America 97 (1) (1995) 680–683.
A. Surlykke, C. F. Moss, Echolocation behavior of big brown bats, Eptesicus fuscus, in the field and the laboratory., The Journal of the Acoustical Society of America 108 (2000) 2419–2429, ISSN 0001-4966.
S. Hoffmann, L. Baier, F. Borina, G. Schuller, L. Wiegrebe, U. Firzlaff, Psychophysical and neurophysiological hearing thresholds in the bat Phyllostomus discolor, Journal of Comparative Physiology A 194 (1) (2008) 39–47.
K. Ubernickel, M. Tschapka, E. K. V. Kalko, Flexible echolocation behavior of trawling bats during approach of continuous or transient prey cues., Front Physiol 4 (2013) 96.
M. L. Melcón, A. Denzinger, H.-U. Schnitzler, Aerial hawking and landing: approach behaviour in Natterer's bats, Myotis nattereri (Kuhl 1818)., J Exp Biol 210 (Pt 24) (2007) 4457–4464.
N. P. Giannini, F. V. Brenes, Flight Cage Observations of Foraging Mode in Phyllostomus discolor, P. hastatus, and Glossophaga commissarisi 1, Biotropica 33 (3) (2001) 546–550.
H. Aldridge, Turning flight of bats., The Journal of Experimental Biology 128 (1987) 419, ISSN 0022-0949.
H. Mittelstaedt, M.-L. Mittelstaedt, Homing by path integration, in: Avian navigation, Springer, 290–297, 1982.
V. Seguinot, Cattet, Benhamou, Path integration in dogs., Anim Behav 55 (4) (1998) 787–797, URL http://dx.doi.org/10.1006/anbe.1997.0662.
M. Lappe, M. Stiels, H. Frenz, J. M. Loomis, Keeping track of the distance from home by leaky integration along veering paths., Exp Brain Res 212 (1) (2011) 81–89.
S. Sterbing-D'Angelo, M. Chadha, C. Chiu, B. Falk, W. Xian, J. Barcelo, J. M. Zook, C. F. Moss, Bat wing sensors support flight control., Proc Natl Acad Sci U S A 108 (27) (2011) 11291–11296.
J. M. Loomis, R. L. Klatzky, R. G. Golledge, J. W. Philbeck, Wayfinding behavior: Cognitive mapping and other spatial processes, chap. Human navigation by path integration, JHU Press,, 125–151, 1999.
H. Wolf, Odometry and insect navigation, The Journal of Experimental Biology 214 (10) (2011) 1629–1641.
M. Müller, R. Wehner, Path integration in desert ants, Cataglyphis fortis., Proceedings of the National Academy of Sciences of the United States of America 85 (July) (1988) 5287–5290, ISSN 0027-8424.
V. Séguinot, R. Maurer, A. S. Etienne, Dead reckoning in a small mammal: the evaluation of distance, Journal of Comparative Physiology A 173 (1) (1993) 103–113, ISSN 03407594.
G. Wyeth, M. Milford, R. Schulz, J. Wiles, The RatSLAM project: robot spatial navigation, in: J. L. Krichmar, H. Wagatsuma (Eds.), Neuromorphic and Brain-Based Robots, Cambridge

University Press, ISBN 9780511994838, 87–108, cambridge Books Online, 2011.

G. Wyeth, M. Milford, Spatial cognition for robots, Robotics & Automation Magazine, IEEE 16 (3) (2009) 24–32.

A. Myronenko, X. Song, Point set registration: Coherent point drift, Pattern Analysis and Machine Intelligence, IEEE Transactions on 32 (12) (2010) 2262–2275.

J. Steckel, A. Boen, D. Vanderelst, H. Peremans, EMFit based Ultrasonic Phased Arrays with evolved Weights for Biomimetic Target Localization, in: 17th IEEE International Symposium on the Applications of Ferroelectrics, 2008.

M. Milford, R. Schulz, Principles of goal-directed spatial robot navigation in biomimetic models, Philosophical Transactions of the Royal Society B: Biological Sciences 369 (1655).

P. Veelaert, H. Peremans, Flexibility maps: A formalisation of navigation behaviours, Robotics and autonomous systems 27 (3) (1999) 151–169.

Z. Kong, N. Fuller, S. Wang, K. Özcimder, E. Gillam, D. Theriault, M. Betke, J. Baillieul, Perceptual Modalities Guiding Bat Flight in a Native Habitat, Scientific Reports 6 (February) (2016) 27252, ISSN 2045-2322, URL http://www.nature.com/articles/srep27252.

A. Cheung, M. Collett, T. S. Collett, A. Dewar, F. Dyer, P. Graham, M. Mangan, A. Narendra, A. Philippides, W. Stürzl, et al., Still no convincing evidence for cognitive map use by honeybees, Proceedings of the National Academy of Sciences 111 (42) (2014) E4396–E4397.

R. Maurer, V. Séguinot, What is modelling for? a critical review of the models of path integration, Journal of Theoretical Biology 175 (1995) 457–475, ISSN 00225193, URL http://www.sciencedirect.com/science/article/B6WMD-45R8FW2-2V/2/90ab5bb694ba5e34587e69bc7b255d64.

S. D. Moeser, Cognitive mapping in a complex building, Environment and Behavior 20 (1) (1988) 21–49.

Appendix A. Supporting material

Appendix A.1. Simulation the echo interference

Equation 3 does not take into account the interference between echoes. For a certain proportion of emitted calls, interference would cause the relative strengths of L_r and L_l to change. Hence, to take this phenomenon into account, we simulated the inference between echoes to estimate the probability of the relative strength of L_r and L_l being changed due to interference.

We generated impulse responses consisting of n echoes, with $n \in [2, 10]$. As our model only takes into account echoes arriving up to 1 ms after the first echo, the length of the impulse responses was set to 1 ms. The amplitude (in Decibels) for each echo i in the impulse response was set according to equation 2 with $r_i \sim \mathcal{U}(r_1, r_1 + 0.17)$. For each generated impulse response, the distance of the first echo r_1 was chosen from a uniform distribution, $r_1 \sim \mathcal{U}(1, 10)$. The azimuth angle α for each echo was drawn from the interval $[-90, 90]$, i.e., $\alpha_i \sim \mathcal{U}(-90, 90)$. For each replication, an impulse response was generated for the left and the right ear by using the head related transfer function of the left and the right ear, respectively.

Both the impulse response for the left and the right ear were convolved with a frequency modulated call sweeping from 100 kHz to 45 kHz in 3 ms. This

resulted in an echo signal for the left and the right ear. Next, both signals were processing using a model of the auditory periphery of the bat as formulated by Wiegrebe (2008).

In brief, the model consists of a Gammatone filterbank with central frequencies ranging from 30 kHz to 100 kHz in steps of 5 kHz. Subsequently, each channel is exponentially compressed (using an exponent value of 0.4) and low-pass filtered (1 kHz cut-off, 12 dB slope per octave). The cochleogram returned by the model was dechirped by shifting each frequency channel in time (zero-padding at the end) such that the maximum activation, corresponding to the pick up of the emitted signal, is aligned across frequency channels. In the model formulated by Wiegrebe (2008) a similar operation is performed by means of a channel-wise normalised autocorrelation between call and echoes. Next, dechirped cochleogram was averaged across frequencies. Finally, The output of the auditory model for each ear was summed to obtain M_l and M_r for the left and the right ear respectively.

Estimating the probability of the relative strengths of L_r and L_l being changed due to interference was done by assessing the proportion of replication for which the relative strength of L_r and L_l did not correspond to the relative strength of M_r and M_l. In other words, the probability $p(n)$ was given by,

$$P(n) = P_n\Big((L_r < L_l \vee M_r > M_l) \wedge (L_r > L_l \vee M_r < M_l)\Big) \tag{A.1}$$

The number of echoes in the impulse response was varied from 2 to 5. For each value of n, 2500 impulse responses were generated. Figure A.13 depicts the resulting $P(n)$ as a function of the number of echoes in the impulse responses. We fitted a quadratic function to the results of the simulation and used to determine the value of $P(n)$ for at each call in the simulations reported in the main text.

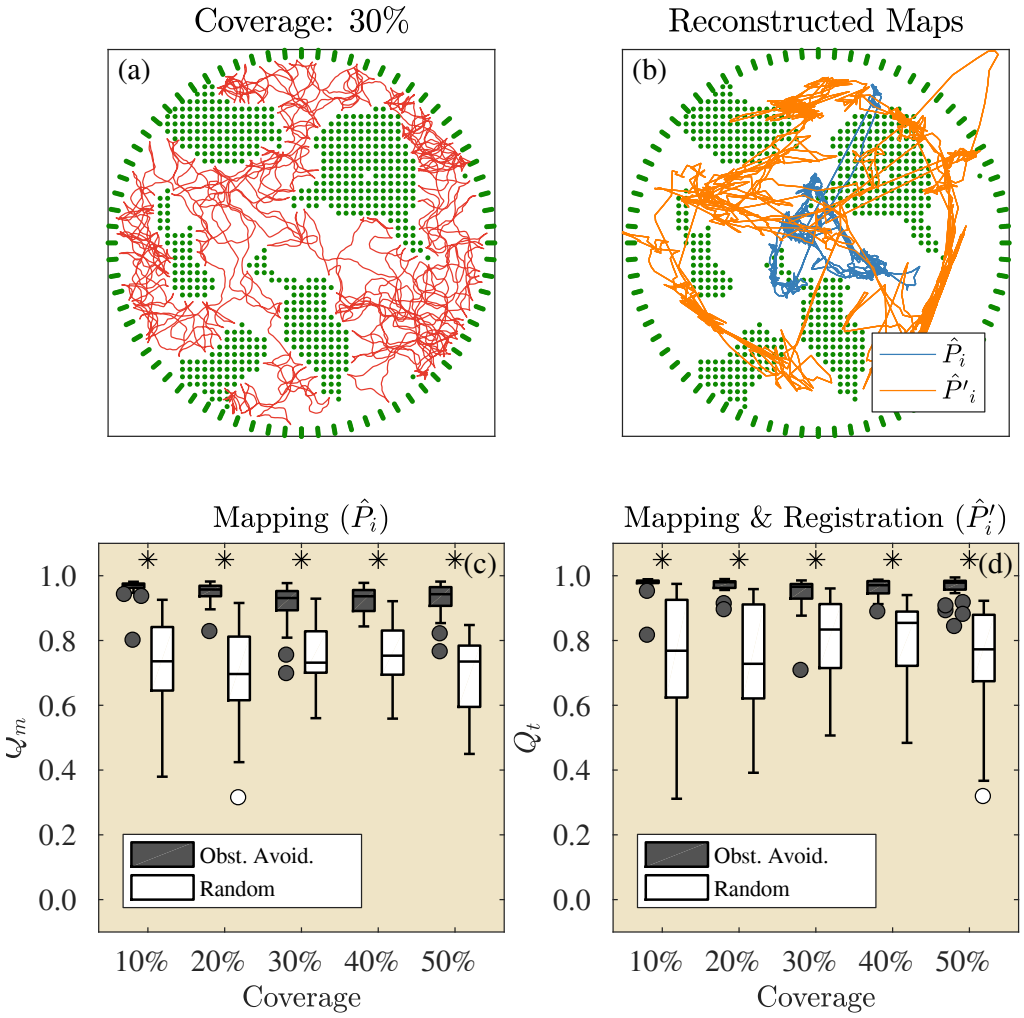

Figure 9: (a) Example of a flight path based on random exploration in an arena with a coverage of 30%. (b) The mapping resulting from the flight path depicted in panel (a). Both the reconstruction based on SLAM alone (metric map) and SLAM and a non-rigid transformation (topological map) are depicted. (c) Boxplots of the map quality Q_m (eq. 21) obtained using the SLAM algorithm based on either random flight paths or flight paths obtained by the obstacle avoidance algorithm. (d) Same as (c), but for the SLAM algorithm followed by a non-rigid transformation, i.e., Q_t (eq. 22). The boxplots are based on 25 replications. Asterisks above a box indicates a significant difference between the results for the random exploration and exploration based on obstacle avoidance (Kruskal-Wallis test, $p < 0.01$).

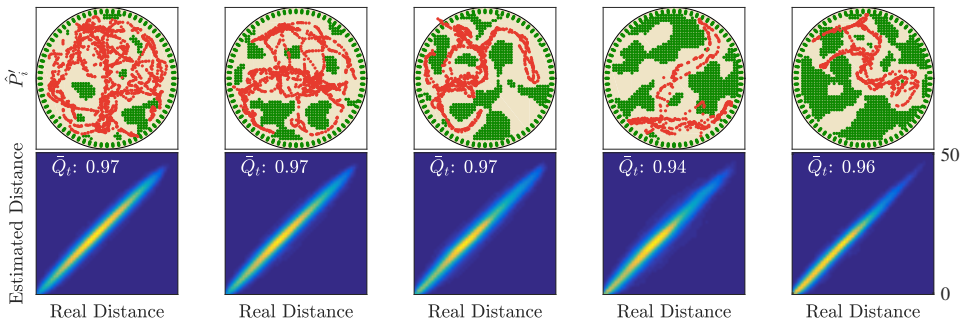

Figure 10: Examples of topological maps. Top row: Estimated positions of each visited place (i.e., the locations $\hat{P'}_i$) using the mapping SLAM algorithm. In addition, the locations have been registered to the real locations $P_i^\star$ by means of a non-rigid transformation. bottom row: histograms showing the correspondence between the distances as estimated using both the SLAM algorithm and a non-rigid transformation ($\hat{P'}_i$) and the real distances (based on $P_i^\star$). These histograms have been calculated using the 25 replications for each coverage level. The mean correlation between the real and estimated distances is given in each panel

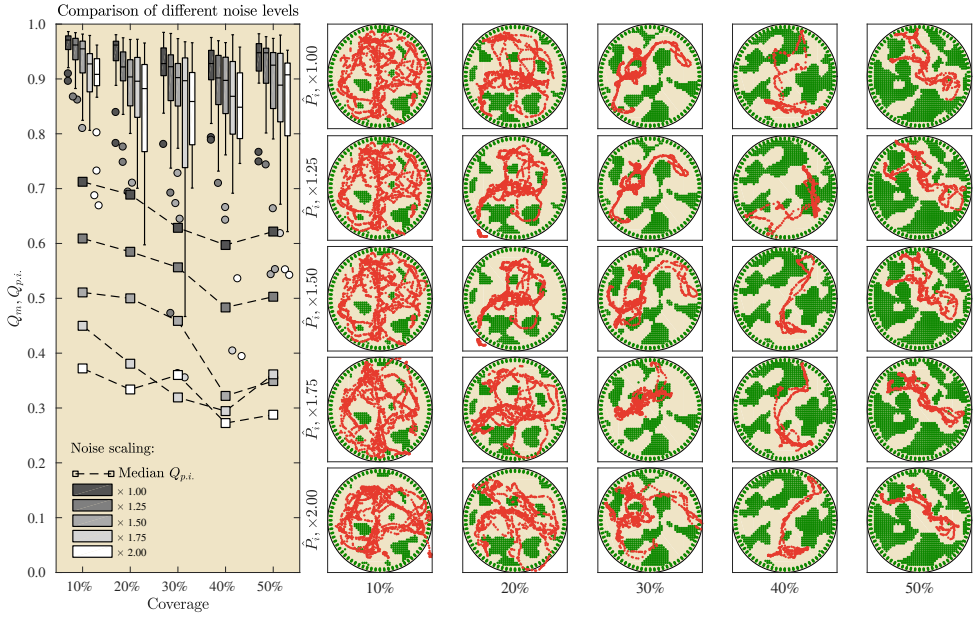

Figure 11: Results of the sensitivity analysis. Left: comparison of the metric map quality Q_m for five noise levels. For each noise level, the values of the noise parameters $\sigma_{\varepsilon_\theta}$, σ_{ε_s} and α were scaled concurrently. The plot also depicts the median map quality resulting from using path integration only, i.e. $Q_{p.i}$. Right: Examples of reconstructed maps for each noise level and the five coverage levels.

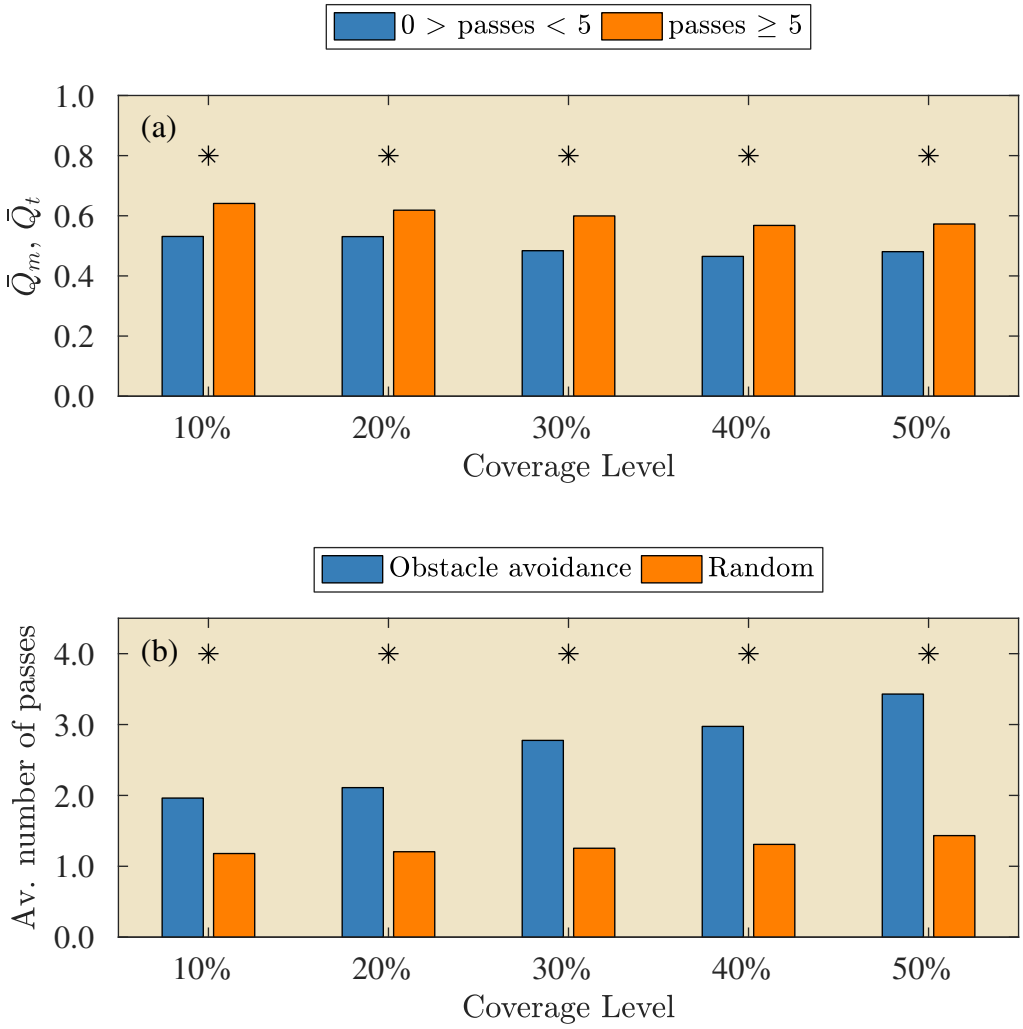

Figure 12: Evaluation of the number of passes between pairs of positions i and j. (a) Average quality metrics (eq. 21 and 22) for the positions i and j as a function of the number of passes between these positions (blue: less than 5 passes; orange: five or more passes). (b) The average number of passes between positions i and j for replications in which the bat was steered either using the obstacle avoidance algorithm or a random motion. A star (★) indicates a significant difference $p < 0.01$.

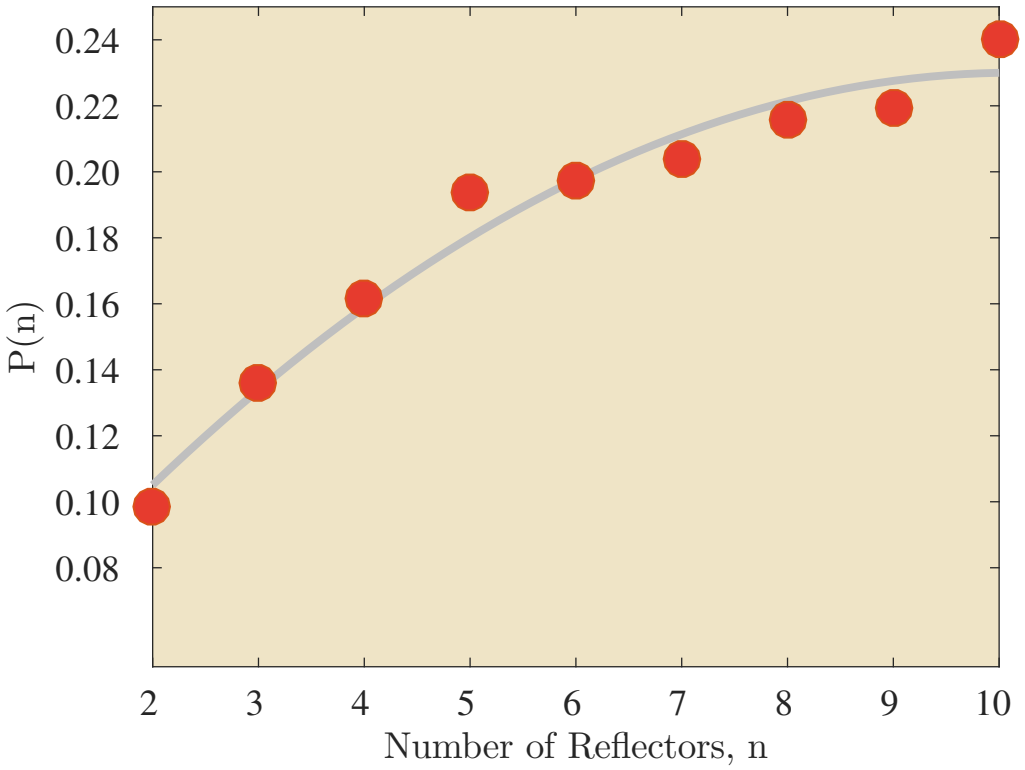

Figure A.13: The probability $P(n)$ as a function of n. The red markers represent the simulation results. The line depicts a quadratic equation fitted to the data. This function was used to determine the values of $P(n)$ used in the simulations reported in the main text.